

THE ABSOLUTE FLUX DISTRIBUTION OF LDS749B

R. C. Bohlin¹ & D. Koester²

bohlin@stsci.edu

ABSTRACT

Observations from the Space Telescope Imaging Spectrograph define the flux of the DBQ4 star LDS749B from 0.12–1.0 μm with an uncertainty of $\sim 1\%$ relative to the three pure hydrogen WD primary *HST* standards. With $T_{\text{eff}} = 13575\text{ K}$, $\log g = 8.05$, and a trace of carbon at $< 1 \times 10^{-6}$ of solar, a He model atmosphere fits the measured STIS fluxes within the observational noise, except in a few spectral lines with uncertain physics of the line broadening theory. Upper limit to the atmospheric hydrogen and oxygen fractions by number are 1×10^{-7} and 7×10^{-10} , respectively. The excellent agreement of the model flux distribution with the observations lends confidence to the accuracy of the modeled IR fluxes beyond the limits of the STIS spectrophotometry. The estimated precision of $\sim 1\%$ in the predicted IR absolute fluxes at 30 μm should be better than the model predictions for Vega and should be comparable to the absolute accuracy of the three primary WD models.

Subject headings: stars: atmospheres — stars: fundamental parameters — stars: individual (LDS749B) — techniques: spectroscopic

1. Introduction

The DBQ4 star LDS749B (WD2129+00) has long been considered for a flux standard (e.g., Bohlin et al. 1990). To establish the flux on the *Hubble Space Telescope* (*HST*) white dwarf (WD) flux scale, STIS spectrophotometry was obtained in 2001–2002. The virtues of LDS749B as a flux standard include an equatorial declination and a significantly cooler flux distribution than the 33000–61000 K primary DA standards GD71, GD153, and G191B2B. Full STIS wavelength coverage is provided from 0.115–1.02 μm , and the peak in the SED

¹Space Telescope Science Institute, 3700 San Martin Drive, Baltimore, MD 21218

²Institut für Theoretische Physik und Astrophysik, Universität Kiel, 24098 Kiel, Germany

is near 1900 Å. At $V = 14.674$ (Landolt & Uomoto 2007), LDS749B is among the faintest *HST* standards and is suitable for use with larger ground-based telescopes and with the more sensitive *HST* instrumentation, such as the ACS/SBC and COS. The bulk of the STIS data was obtained as part of the FASTEX (Faint Astronomical Sources Extention) program. Finding charts appear in Turnshek et al. (1990) and in Landolt & Uomoto (2007); but there is a large proper motion of 0.416 and 0.034 arcsec/yr in right ascension and declination, respectively.

The absolute flux calibration of *HST* instrumentation is based on models of three pure hydrogen WD stars GD71, GD153, and G191B2B (Bohlin 2000; Bohlin, Dickenson, & Calzetti 2001; Bohlin 2003). In particular, the NLTE model fluxes produced by the TLUSTY code (Hubeny & Lanz 1995) determine the shape of the flux distributions using the known physics of the hydrogen atom and of stellar atmospheres. If there are no errors in the basic physics used to determine the stellar temperatures and gravities from the Balmer line profiles, then the uncertainty of 3000 K for the effective temperature of G191B2B means that the relative flux should be correct to better than 2.5% from 0.13 to 1 μm and to better than 1% from 0.35 to 1 μm .

A model that matches the observations serves as a noise free surrogate for the observational flux distribution and provides a reliable extrapolation beyond the limits of the observations for use as a calibration standard for *JWST*, *Spitzer*, and other IR instrumentation. Currently, the best IR absolute flux distributions are found in a series of papers from the epic and pioneering work of M. Cohen and collaborators, i.e., the Cohen-Walker-Witteborn (CWW) network of absolute flux standard (e.g., Cohen, Wheaton, & Megeath 2003; Cohen 2007). The CWW IR standard star fluxes are all ultimately based on models for Vega and Sirius (Cohen et al. 1992). More recently, Bohlin & Gilliland (2004) observed Vega and published fluxes on the *HST*/STIS WD flux scale. A small revision in the STIS calibration resulted in excellent agreement of the STIS flux distribution with a custom made Kurucz model with $T_{\text{eff}} = 9400$ K (Bohlin 2007), which is the same T_{eff} used for the Cohen et al. (1992) Vega model.

The model presented here for LDS749B and archived in the CALSPEC database¹ should have a better precision than the Kurucz $T_{\text{eff}} = 9400$ K model for Vega, especially beyond ~ 12 μm , where the Vega’s dust disk becomes important (Engleke, Price, & Kraemer 2006). Vega is also a pole-on rapid rotator, which may also cause IR deviations from the flux for a single temperature model. Our modeled flux distribution for LDS749B should have an

¹The absolute spectral energy distributions discussed in this paper are available in digital form at <http://www.stsci.edu/hst/observatory/cdbs/calspec.html>.

accuracy comparable to the pure hydrogen model flux distributions for the primary WD standards GD71, GD153, and G191B2B.

2. The Model

A helium model atmosphere flux distribution for LDS749B is calculated with the LTE code of Koester (e.g., Castanheira et al. 2006) for $T_{\text{eff}} = 13575$ K and $\log g = 8.05$. At such a cool temperature, the differences between LTE and NLTE in the continuum flux distributions should be $<0.1\%$ from the far-UV to the IR. For example for a pure hydrogen DA, the difference between the continua of a hot 40,000 K LTE/NLTE pair of models is 1% between 0.1–2.5 μm . The same maximum difference at 20,000 K is only 0.3%. Napiwotzki (1997) did not discuss pure He models but concludes that NLTE effects tend to become smaller with lower effective temperature. For cool DA WDs, Koester et al. (1998) show that the only NLTE effect that approaches 1% is a deeper line core of $\text{H}\alpha$. The matter densities in helium-rich white dwarfs are significantly higher, leading to a higher ratio of collisional versus radiative transitions between atomic levels. The larger importance of collisions increases the tendency towards LTE occupation numbers because of the robust Maxwell distribution of particle velocities.

The $T_{\text{eff}} = 13575$ K is higher than the $T_{\text{eff}} = 13000$ K published for LDS749B (alias G26–10) in Castanheira et al. (2006), because only UV spectra of lower precision (*IUE* heritage) were used in that analysis. Voss et al. (2007) found $T_{\text{eff}} = 14440$ K with large uncertainty, because only line profiles in the optical range were used and $\log g$ had to be assumed. A trace of carbon at 10^{-6} of the solar C/He ratio is included, i.e. the C/He number ratio is 3.715×10^{-9} . The model mass is $0.614 M_{\odot}$ and the stellar radius is $0.01224 R_{\odot}$, which corresponds to a distance of 41 pc for the measured STIS flux.

The line broadening theory for the He lines combines van der Waals, Stark, and Doppler broadening to make a Voigt profile. However, the Stark broadening uses a simple Lorentz profile with width and shift determined from the broadening data in Griem (1964), instead of the elaborate calculations of Beauchamp et al. (1997). The Griem method is computationally much faster, and data are available for more lines than are calculated by Beauchamp et al.

The fit of the higher series He lines is much improved, if the neutral-neutral interaction is decreased in comparison to the original formalism of the Hummer-Mihalas occupation probabilities. A similar effect was noticed by Koester et al. (2005), and our model uses the same value of the quenching parameter that Koester et al. derived ($f = 0.005$). The model wavelengths are all on a vacuum scale.

3. STIS Spectrophotometry

The sensitivities of the five STIS low dispersion spectrophotometric modes have been carefully tracked since the STIS commissioning in 1997. After correcting for changing sensitivity with time (Stys, Bohlin, & Goudfrooij 2004) and for charge transfer efficiency (CTE) losses for the three STIS CCD spectral modes (Bohlin & Goudfrooij 2003; Goudfrooij et al. 2006), STIS internal repeatability is often better than 0.5% (Bohlin 2003). Thus, *HST*/STIS observations of LDS749B provide absolute spectrophotometry with a precision that is superior to ground based flux measurements, which require problematic corrections for atmospheric extinction.

Observations with a resolution $R = 1000$ – 1500 in four STIS modes from 1150–1710 Å (G140L), 1590–3170 Å (G230L), 2900–5690 Å (G430L), and 5300–10200 Å (G750L) were obtained in 2001–2002. Earlier observations of LDS749B in 1997 to test the time-tagged mode were unsuccessful. Two observations in the CCD G230LB mode overlap the wavelength coverage of the MAMA G230L but are too noisy to include in the final combined absolute flux measurement from the other four modes. Table 1 summarizes the individual observations used for the final combined average, along with the unused G230LB data for completeness.

Figure 1 shows the ratios of the three individual G230L and the two G230LB observations to the model fluxes, which are normalized to the STIS flux in the 5300–5600 Å range. The excellent repeatability of STIS spectrophotometry over broad bands is illustrated and the global average ratio over the 1750–3000 Å band pass is written in each panel. This ratio is unity to within 0.3%, even for the shorter CCD G230LB exposures despite their almost $3\times$ higher noise level and CTE corrections. The other CCD modes G430L and G750L also require CTE corrections. Repeatability for all the STIS spectral modes is comparable, i.e., the global ratio deviates rarely from unity by more than 0.6%.

The observations in each of the four spectral modes are averaged and the four segments are combined. This composite standard star spectrum extends from 1150–10226 Å and can be obtained at <http://www.stsci.edu/hst/observatory/cdb/calspec.html/> along with the remainder of the *HST* standard star library (Bohlin, Dickenson, & Calzetti 2001). This binary fits table named *lds749b_stis_001.fits* has 3666 wavelength points and seven columns. An ascii file of the flux distribution in Table 2 is available via the electronic version of this paper. Table 2 contains the wavelength in Å and the flux in $\text{erg cm}^{-2} \text{s}^{-1} \text{Å}^{-1}$ in the first two columns, while columns 3–4 are the Poisson and systematic uncertainty estimates in flux units, respectively. Column 5 is the FWHM of the resolution in Å. The *fits* version has two more columns than the ascii version: Column 6 is a data-quality flag, where one is good and zero may be poor quality. The seventh column is the exposure time in seconds. The fluxes at the shortest wavelengths below 1160 Å are unreliable because of the steepness of

the sensitivity drop-off.

4. Comparison of the Observations with the Model

4.1. The Continuum

To compare the model and observations, a convenient method of removing the slope of the spectral energy distribution (SED) is to divide both fluxes by the same theoretical model continuum. Small differences between the observations and the model, either in the lines or in the actual continuum, are easily illustrated in such plots. The theoretical continuum contains only continuum opacities with an extrapolation across the He I opacity edges at 2601, 3122, and 3422 Å, in order to avoid discontinuities. Figure 2 shows an overview of the comparison of the STIS fluxes with the model after division of both SEDs by this same smooth line-and-edge-free continuum. The mean continuum level of the data between the absorption lines agrees with the model within $\sim 1\%$ almost everywhere.

The most significant deviation of the data from the model is in the broad 1400–1550 Å region, where each of the three spectra comprising the G140L average have 350,000 photoelectron events in this 150 Å band. The background level is $<0.1\%$ of the net signal, so that neither counting statistics nor background subtraction error could cause the observed $\sim 1.5\%$ average disparity. Of the five low dispersion modes, G140L shows the worst photometric repeatability of individual spectra in broad bands of $\sigma \sim 0.6\%$. The three individual spectra comprising the G140L average do show occasional 2–3 σ broadband dips within their 550 Å coverage region; but the probability of such a large excursion as 1.5% in their average is extremely unlikely at any particular wavelength. However, the probability is much greater that such a large excursion could occur in some 150 Å band. Individual G140L spectra of the monitoring standard GRW+70°5824 often show a broad region differing by 1–2% from the average. The cause of such excursions could be flat field errors, temporal instabilities in the flat field, or other detector effects that might make the flat field inapplicable to a narrow spectral trace.

4.1.1. Uncertainties in T_{eff} and $\log g$

The uncertainty in the model T_{eff} is determined by the uncertainty in the slope of the UV flux distribution. For a constant $\log g$ model that is cooler or hotter by 50 K and normalized to the measured 5300–5600 Å flux, there are increasing differences with the data from 1% near 2000 Å to 2% at the shorter wavelengths. Such a large change in the modeled

continuum level in Figure 2 (red line) is inconsistent with the STIS flux (black line). This 50 K uncertainty of the model T_{eff} is an internal uncertainty relative to the temperatures of the primary WD standards GD71, GD153, and G191B2B. If a re-analysis of the Balmer lines in these primary DA standards produces a systematic shift in the temperature scale, this shift would be reflected in a revised T_{eff} for LDS749B that is independent of the 50 K internal uncertainty. A 50 K temperature difference causes a $<0.5\%$ flux change in the IR longward of $1 \mu\text{m}$.

To estimate the uncertainty in $\log g$, models are computed at the 13575 K baseline temperature but with an increment in $\log g$. Positive and negative increments produce nearly mirror image changes in the flux distribution. For a decrease of 0.7 in $\log g$, the flux decreases by a nearly uniform 1.5% below 3600 Å after normalizing to unity in the 5300–5600 Å range. Increasing the T_{eff} by the full 50 K uncertainty to 13625 K can compensate for this flux decrease below ~ 2000 Å. However, the +50 K increase compensates little in the 2500–3600 Å range, leaving a disparity of $\sim 1\%$. Because this 2500–3600 Å range includes some of the best S/N STIS data, a 1% disparity establishes the uncertainty of 0.7 dex in $\log g$ as barely compatible with the STIS flux distribution. The IR uncertainty corresponding to this limiting case of $T_{\text{eff}} = 13625$ K and $\log g = 7.35$ is $\sim 1\%$ longward of $1 \mu\text{m}$, because the fractional percent changes in the IR from the higher temperature and from the lower $\log g$ are both in the same direction.

4.1.2. *Interstellar Reddening*

Another source of error in the model T_{eff} is interstellar reddening. The standard galactic reddening curve has a strong broad feature around 2200 Å; and a tiny limit to the extinction $E(B - V)$ is set by the precise agreement of STIS with the model in this region of Figure 2. For the upper temperature limit of $13575 + 50 = 13625$ K, an $E(B - V) = 0.002$ brings the reddened model into satisfactory agreement with STIS. However, for a temperature increment of 100 K and $E(B - V) = 0.004$, the model is $\sim 1\%$ high at 1300 Å and $\sim 1\%$ low at 2200 Å. Thus, for standard galactic reddening, $E(B - V)$ must be less than 0.004, and T_{eff} is less than 13675 K. In this case of T_{eff} and $E(B - V)$ at these allowed limits, the IR flux beyond $1 \mu\text{m}$ is still the same as for the unreddened baseline $T_{\text{eff}} = 13575$ K within 0.5%.

However, Bohlin (2007) presented arguments for reddening with a weak 2200 Å bump for other lines of sight with tiny amounts of extinction. Reddening curves measured in the SMC (e.g., Witt & Gordon 2000) are missing the 2200 Å feature and can cause larger uncertainty in T_{eff} . Additional evidence for extinction curves more like those in the Magellanic clouds is presented by Clayton et al. (2000) for the local warm intercloud medium, where the

reddening is low. Changes in the shape of the flux distribution after reddening with the SMC curve of Witt and Gordon are similar to the change in shape with T_{eff} . For example, reddening a model with $T_{\text{eff}} = 14130$ K by SMC extinction of 0.015 is required to make an equally unacceptable fit as for 13675 K and galactic extinction of $E(B - V) = 0.004$. In this extreme limiting case of SMC extinction, the IR flux beyond $1 \mu\text{m}$ is still the same within $\sim 1\%$ as for $T_{\text{eff}} = 13575$ K and $E(B - V) = 0$.

Despite small uncertainties in the interstellar reddening and consequent uncertainty in T_{eff} , our modeling technique still predicts the continuum IR fluxes to 1% from $1 \mu\text{m}$ to $30 \mu\text{m}$. Discounting the most pathological case of SMC reddening, the worst far-IR uncertainty is from the combined 50 K temperature and $0.7 \log g$ uncertainties, because the changes in the slope from the visual band normalization region into the IR due to higher temperature and lower $\log g$ are both in the same direction. In the absence of modeling errors or other physical complications like IR excesses from dust rings, the measured fluxes of LDS749B relative to the three primary WDs should be the same as predicted by the relative fluxes of the respective models to a precision of 1% in the IR.

4.2. The Stellar Absorption Lines

4.2.1. Hydrogen

An upper limit on the equivalent width for $\text{H}\alpha$ of $\sim 0.1 \text{ \AA}$ constrains the fraction by number of hydrogen in the atmosphere of LDS749B to $< 1 \times 10^{-6}$ of helium. However, a stricter limit of $< 1 \times 10^{-7}$ is provided by the weak $\text{Ly}\alpha$ line. Because interstellar absorption at $\text{Ly}\alpha$ could be significant, zero hydrogen is consistent with the observations and is adopted for the final best model for LDS749B. After normalization in the V band, the continuum of a model with 1×10^{-7} hydrogen composition and the baseline $T_{\text{eff}} = 13575$ K and $\log g = 8.05$ agrees with the zero hydrogen baseline continuum to $\sim 0.5\%$ from $\text{Ly}\alpha$ to $30 \mu\text{m}$.

4.2.2. Helium

Figure 3 compares the observed HeI lines with the baseline model after correcting the model wavelengths by the radial velocity of -81 km s^{-1} (Greenstein & Trimble 1967). The model is smoothed with a triangular profile of FWHM corresponding to a resolution $R = 1500$ for the MAMA spectra shortward of 3065 \AA and to $R = 1000$ for the CCD spectra longward of 3065 \AA . In general, the model underestimates the line strengths, even for the quenching of the neutral-neutral interactions with $f = 0.005$. There is a suggestion of some systematic

asymmetry with stronger absorption in the short wavelength side of the line profile. This asymmetry could be in the STIS line spread function (LSF); or perhaps, a more exact treatment of the Stark line broadening theory would reproduce the observed asymmetries.

4.2.3. Carbon

With a C/He ratio of $<1 \times 10^{-6}$ solar, i.e. a C/He number ratio of 3.715×10^{-9} , the modeled C I and C II lines reproduce the observations within the observational noise, as shown in Figure 4. In particular, the agreement of the modeled C I(1329)/C II(1335) line ratio with the observed ratio means that the carbon ionization ratio corresponds to the photospheric temperature of the star. With this small amount of carbon, the spectral classification of LDS749B should more properly be DBQ (Wesemael et al. 1993).

4.2.4. Oxygen

The oxygen triplet at 1302.17, 1304.87, and 1306.04 Å constrains the fraction of oxygen in the LDS749B atmosphere. This triplet absorption feature extends over 4 Å or about seven STIS pixels; but no obvious absorption feature appears above the noise level. After binning the STIS data by seven pixels, the rms noise in the 1300 Å region is 0.8%. The corresponding 3σ upper limit to the equivalent width is 0.10 Å, which implies an upper limit to the atmospheric oxygen fraction by number of 7×10^{-10} of helium.

5. Conclusion

In the absence of any interstellar reddening, a helium model with $T_{\text{eff}} = 13575 \text{ K} \pm 50$, $\log g = 8.05 \pm 0.7$, and a trace of carbon at $<1 \times 10^{-6}$ of solar fits the measured STIS flux distribution for LDS749B. The noise-free, absolute flux distribution from the model after normalization to the observed broadband visual flux is preferred for most purposes. This normalized model SED is a high fidelity far-UV to far-IR calibration source; and the flux distribution is available via Table 3 in the electronic version of the *Journal*. Both the observed flux distribution and the modeled fluxes are also available from the CALSPEC database.²

²<http://www.stsci.edu/hst/observatory/cdbs/calspec.html/>.

Primary support for this work was provided by NASA through the Space Telescope Science Institute, which is operated by AURA, Inc., under NASA contract NAS5-26555. Additional support came from DOE through contract number C3691 from the University of California/Lawrence Berkeley National Laboratory. This research has made use of the SIMBAD database, operated at CDS, Strasbourg, France.

REFERENCES

- Beauchamp, A., Wesemael, F., & Bergeron, P. 1997, *ApJS*, 108, 559
- Bohlin, R. C. 2000, *AJ*, 120, 437
- Bohlin, R. C. 2003, in 2002 HST Calibration Workshop, eds. S. Arribas, A. Koekemoer, & B. Whitmore, (Baltimore: STScI), p. 115
- Bohlin, R. C. 2007, in The Future of Photometric, Spectrophotometric, and Polarimetric Standardization, ASP Conf. Series, Vol. 364, p. 315 ed. C. Sterken; also astro-ph 0608715
- Bohlin, R. C., Dickinson, M. E., & Calzetti, D. 2001, *AJ*, 122, 2118
- Bohlin, R. C., & Gilliland, R. L. 2004, *AJ*, 127, 3508
- Bohlin, R., & Goudfrooij, P. 2003, Instrument Science Report, STIS 03-03, (Baltimore: STScI)³
- Bohlin, R. C., Harris, A. W., Holm, A. V., & Gry, C. 1990, *ApJS*, 73, 413
- Castanheira, B., Kepler, S., Handler, G., & Koester, D. 2006, *A&A*, 450, 331
- Clayton, G., Gordon, K., & Wolff, M. 2000, *ApJS*, 129, 147
- Cohen, M. 2007, in The Future of Photometric, Spectrophotometric, and Polarimetric Standardization, ASP Conf. Series, Vol. 364, p. 333, ed. C. Sterken
- Cohen, M., Walker, R. G., Barlow, M. J., & Deacon, J. R. 1992, *AJ*, 104, 1650
- Cohen, M., Wheaton, W., & Megeath, S. 2003, *AJ*, 126, 1090
- Engleke, C., Price, S., & Kraemer, K. 2006, *AJ*, 132, 1445
- Goudfrooij, P., Bohlin, R., Maíz-Apellániz, J., & Kimble, R. 2006, *PASP*, 118, 1455
- Griem, H. R. 1964, *Plasma Spectroscopy*, (New York: McGraw-Hill)
- Greenstein J. L., & Trimble V. L. 1967, *ApJ*, 149, 283
- Hubeny, I., & Lanz, T. 1995, *ApJ*, 439, 875

³This STScI internal document can be found at: <http://www.stsci.edu/hst/stis/documents/isrs/>.

- Koester, D., Dreizler, S., Weidemann, V., & Allard, N. F. 1998, *A&A*, 338, 612
- Koester, D., Napiwotzki, R., Voss, B., Homeier, D., & Reimers, D. 2005, *A&A*, 439, 317
- Landolt, A. U., & Uomoto, A. K. 2007, *AJ*, 133, 768
- Napiwotzki, R. 1997, *A&A*, 322, 256
- Stys, D. J., Bohlin, R. C. & Goudfrooij, P. 2004, Instrument Science Report, STIS 2004-04, (Baltimore: STScI)⁴
- Turnshek, D. A., Bohlin, R. C., Williamson, R. L., Lupie, O. L., Koornneef, J., & Morgan D. H. 1990, *AJ*, 99, 1243
- Voss, B., Koester, D., Napiwotzki, R., Christlieb, N., & Reimers, D. 2007, *A&A*, 470, 1079
- Wesemael, F, et al. 1993, *PASP*, 105, 761
- Witt, A., & Gordon, K. 2000, *ApJ*, 528, 799

⁴This STScI internal document can be found at: <http://www.stsci.edu/hst/stis/documents/isrs/>.

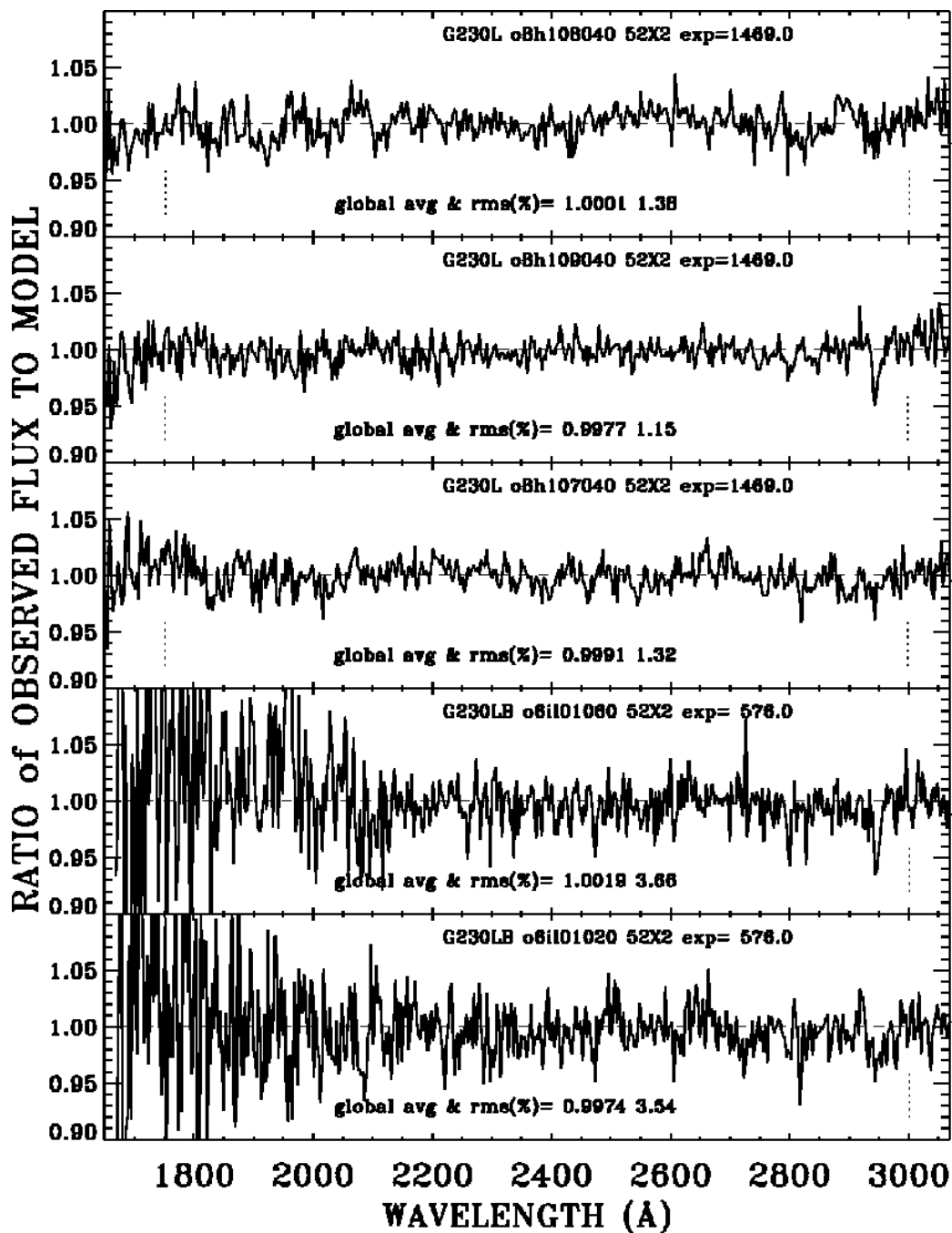


Fig. 1.— Ratio of individual STIS observations to the LDS749B model fluxes. Both the data and the model are binned to the ~ 2 pixel resolution of STIS before dividing. The global average and rms for the range between the vertical dotted lines are written in each panel along with the identifying information for each observation: spectral mode, root name, aperture, and exposure time in seconds. The noisier, short-exposure CCD mode G230LB data shown in the bottom two panels are not used in the final average of the observations.

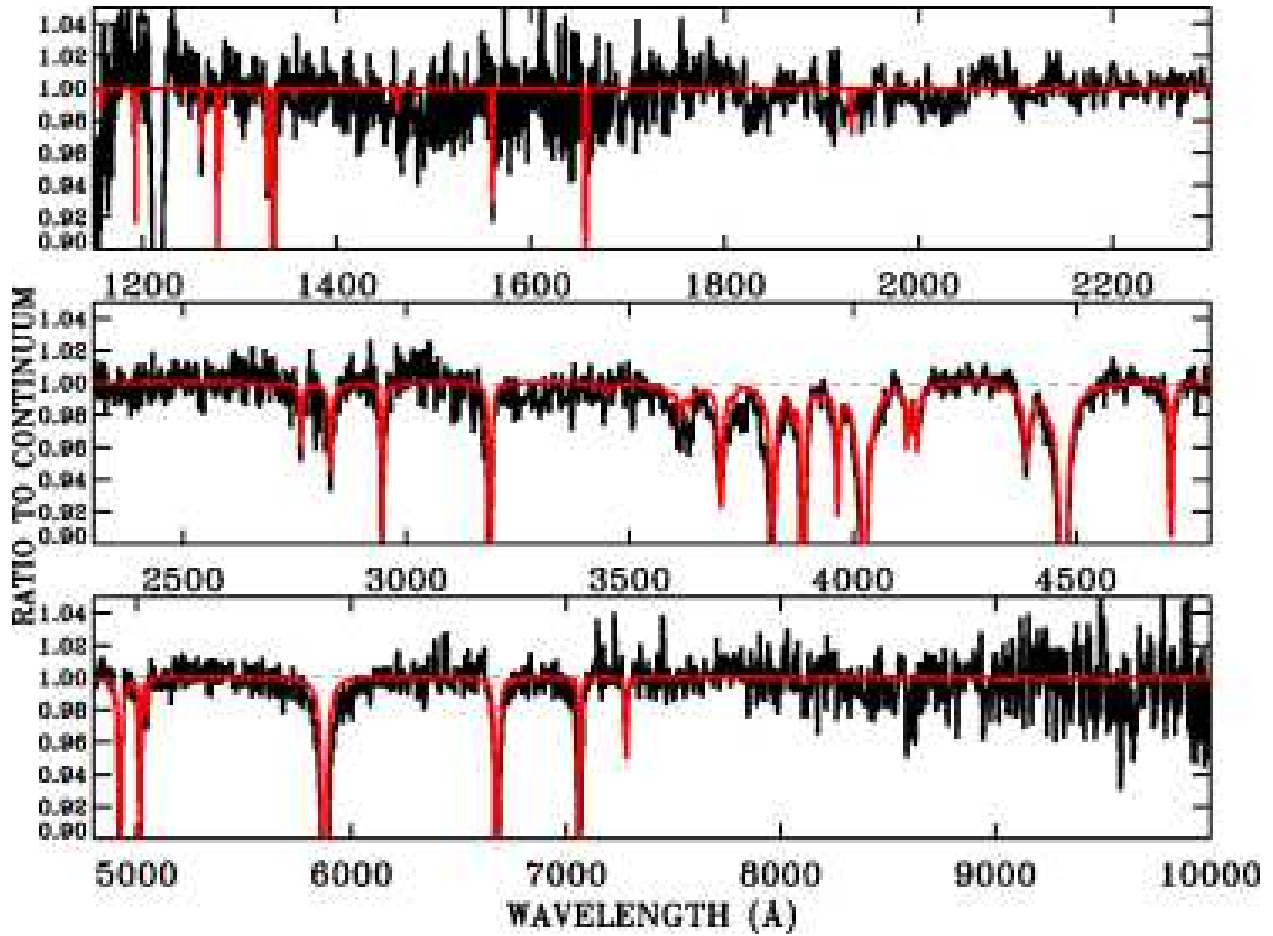


Fig. 2.— Comparison of the STIS observations with the model after scaling both SEDs by the same edge-free theoretical model continuum. Both the model and its theoretical continuum flux distributions are normalized to match the average STIS flux in the 5300–5600 Å region. The model flux is smoothed to the approximate STIS resolution of $R = 1500$ for the MAMA spectra (shortward of 3065 Å) and to $R = 1000$ for the CCD spectra (longward of 3065 Å). A thin dashed line marks the unity level.

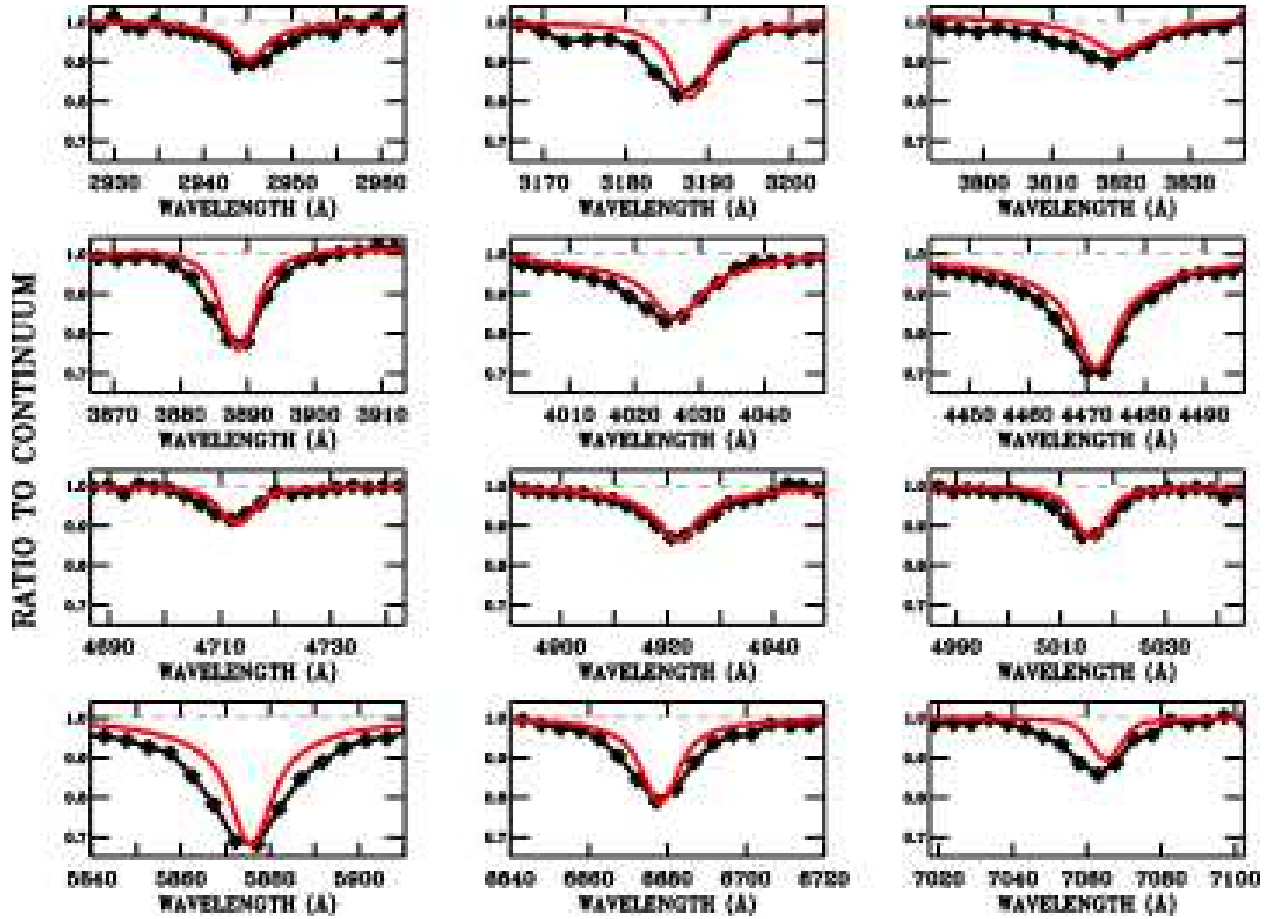


Fig. 3.— The 12 strongest He I lines in LDS749B as in Figure 2, except on an expanded wavelength scale.

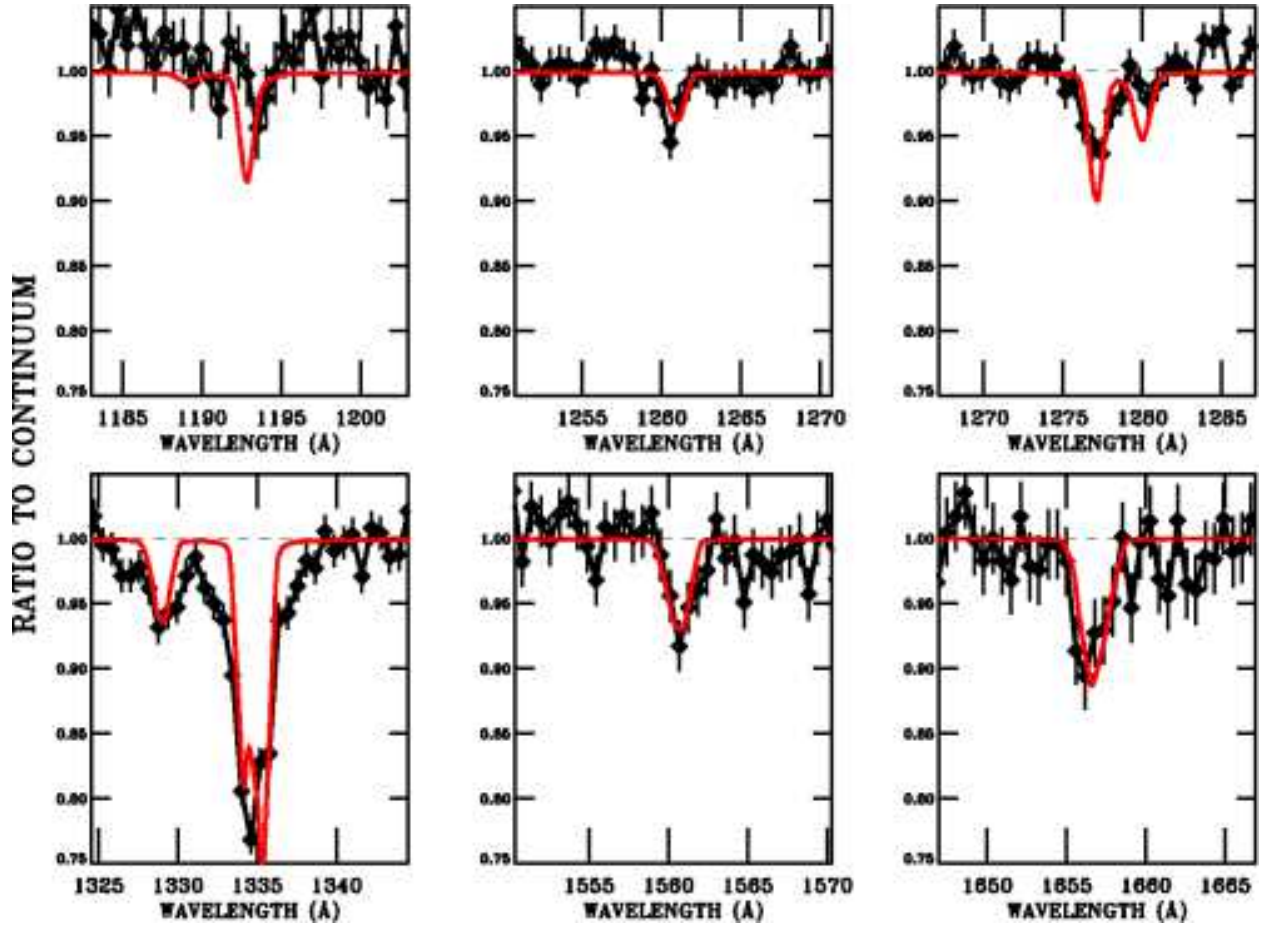


Fig. 4.— Carbon lines in LDS749B as in Figure 2, except on an expanded wavelength scale. The error bars are 1σ .

Table 1. Journal of Observations

Rootname	Mode	Aperture	Date	Exptime(s)
O6IL01020	G230LB	52×2	2001-07-13	576
O6IL01030	G430L	52×2	2001-07-13	619
O6IL01040	G750L	52×2	2001-07-13	1380
O6IL01060	G230LB	52×2	2001-07-13	576
O6IL01070	G430L	52×2	2001-07-13	576
O6IL01080	G750L	52×2	2001-07-13	1584
O8H107010	G140L	52×2	2002-09-01	2266
O8H107020	G430L	52×2	2002-09-01	400
O8H107030	G430L	52×2E1	2002-09-01	400
O8H107040	G230L	52×2	2002-09-01	1469
O8H108010	G140L	52×2	2002-10-16	2266
O8H108020	G430L	52×2	2002-10-16	400
O8H108030	G430L	52×2E1	2002-10-16	400
O8H108040	G230L	52×2	2002-10-16	1469
O8H109010	G140L	52×2	2002-12-27	2266
O8H109020	G430L	52×2	2002-12-27	400
O8H109030	G430L	52×2E1	2002-12-27	400
O8H109040	G230L	52×2	2002-12-27	1469

Table 2. Measured STIS Absolute Flux Distribution for LDS749B

Wavelength	Flux	Poisson	Systematic	FWHM
1150.31	1.68860e-14	8.09170e-16	1.68860e-16	1.16699
1150.89	1.59170e-14	7.54240e-16	1.59170e-16	1.16687
1151.47	1.51450e-14	7.07050e-16	1.51450e-16	1.16687
1152.06	1.57620e-14	7.02910e-16	1.57620e-16	1.16699
1152.64	1.54940e-14	6.71560e-16	1.54940e-16	1.16699

Note. — The complete version of this table is in the electronic edition of the *Journal*. The printed edition contains only a sample.

Table 3. Model Absolute Flux Distribution for LDS749B

Wavelength	Flux	Continuum
900.000	8.7713311e-15	8.7863803e-15
900.250	8.7785207e-15	8.7950878e-15
900.500	8.7853486e-15	8.8037809e-15
901.000	8.7975857e-15	8.8212095e-15
901.500	8.8064389e-15	8.8386236e-15

Note. — The complete version of this table is in the electronic edition of the *Journal*. The printed edition contains only a sample.